Acta Phys. Hung. A 21/2–4 (2004) 243–248

HEAVY ION
PHYSICS

# Expansion Rates at RHIC

Peter F. Kolb

Department of Physics and Astronomy, SUNY at Stony Brook
Stony Brook, NY 11780, USA

*Received 12 April 2003*

**Abstract.** A detailed description of the temporal evolution of the thermodynamic fields in heavy ion collisions is presented within a hydrodynamic framework. Particular attention is devoted to the evolution of the collective flow fields and their space-time gradients.

*Keywords:* relativistic heavy-ion collisions, hydrodynamic model
*PACS:* 25.75-q, 25.75.Ld, 25.75.Nq

## 1. Introduction and Motivation

Experimental data from RHIC [1], in particular the systematic analysis of anisotropies in the particle spectra, indicate that at high center of mass energies the collision region rapidly thermalizes and for the major part of its evolution subsequently expands according to the laws of ideal hydrodynamics (for a recent review that collects the arguments and references which support this hydrodynamic scenario see [2]). This is an important finding by itself as apparently the generated system spends some time at temperatures above the anticipated QCD transition temperature and evolves according to the pressure, pressure-gradients and thus equation of state of deconfined strongly interacting matter.

Furthermore the hydrodynamic evolution can be used to shed light even onto some microscopic scattering phenomena, such as signals from hard probes which propagate through the hydrodynamically evolving 'background' fields and radiate energy, as well as the late freeze-out dynamics of the reaction. Such probes are significantly dependent on the evolution of the macroscopic fields such as temperature and particle density, but also on the collective flow velocities and their gradients.

We will here give a detailed study of the evolution of these fields. First we investigate a simple analytically accessible parametrization of the flow field and its divergence. Then we will discuss the hydrodynamic evolution of thermodynamic fields in a full hydrodynamic calculation to return later to the collective flow fields and compare to the initial analytic example.

1219-7580/04/ $ 20.00

## 2. Expansion Rate and Dilution Rate

Ideal hydrodynamics incorporates the continuity equations for conserved charges $\partial_\mu n^\mu = 0$ where $n^\mu = n\,u^\mu$ is the current associated with the conserved charge whose density distribution is given by $n(x)$ and $u^\mu(x)$ is the four-velocity of the collective flow field. In ideal hydrodynamics the entropy density is such a conserved quantity. Slightly reshaping the continuity equation leads to the relation

$$\partial_\mu u^\mu = -\frac{1}{n}\, u^\mu \partial_\mu\, n\,. \tag{1}$$

The expression $\partial_\mu u^\mu$ is commonly referred to as *expansion rate*. Considering the trivial condition of vanishing collective flow $u^\mu = (1,0,0,0)$ as is the case in the center of the system due to symmetry, the expansion rate is simply given as $\partial_\mu u^\mu = -\dot{n}/n$, the *dilution rate*. Assuming furthermore a power-law decay of the density $n \sim \tau^{-\alpha}$ as is the case for the three-dimensional Hubble expansion of the Universe ($\alpha = 3$) or the one-dimensional longitudinal Bjorken expansion ($\alpha = 1$) the expansion rate is given by $\partial_\mu u^\mu = \alpha/\tau$ ($\alpha$ is referred to as *expansion parameter*).

Let us now investigate a more general situation, namely a longitudinal Bjorken flow field $v_z = \tanh\eta = z/t$ with a transverse flow component given as $\gamma\, v_T = \tanh(\xi r)$. We will later see that the hydrodynamic calculations in fact suggest such a flow profile at freeze-out with $\xi \approx 0.07$ fm$^{-1}$. It is quickly shown that this flow field leads to an expansion rate

$$\partial_\mu u^\mu = \tau^{-1}\cosh(\xi r) + \xi\cosh(\xi r) + r^{-1}\sinh(\xi r)\,, \tag{2}$$

which in the limit $(r,z) \to 0$ leads to $\partial_\mu u^\mu \to 1/\tau + 2\xi$ as discussed in [3]. Keeping the radial dependence in the expression one finds that the expansion rate increases with radial distance from 0.207 fm$^{-1}$ at $r = 0$ to 0.247 fm$^{-1}$ at $r = 10$ fm (assuming $\tau = 15$ fm/$c$, a typical fireball lifetime). This will become important later in this study.

In the case of such a non-zero transverse flow profile the spatial part of the four product on the right hand side of Eq. (1) does not vanish and the expansion rate is no longer identically equal to the dilution rate. This becomes apparent by assuming a boost invariant distribution of the conserved charge (which means that the charge density only depends on the proper time $\tau = \sqrt{t^2 - z^2}$ and not on the space-time rapidity $\eta$) and describing its dilution locally in terms of a power law such that $n(r,\tau) = n_0(r)(\tau_0/\tau)^\alpha$. It then quickly follows from Eq. (1) that

$$\tau\,\partial_\mu u^\mu = \gamma\left(\alpha - \tau\, v_r \frac{\partial_r n_0(r)}{n_0(r)}\right). \tag{3}$$

As the density is expected to drop with increasing radial distance the last term in the brackets is negative and gives a positive correction to $\alpha$ as does the preceding $\gamma$ factor. It thus follows that in general the expansion rate $\partial_\mu u^\mu$ is greater or equal to the local dilution rate $\alpha/\tau$.

## 3. Time Evolution of Thermodynamic Fields in Central Collisions

We now investigate the evolution of the thermodynamic fields using a hydrodynamic model [4] which explicitly assumes boost invariance throughout the evolution. The initial field configuration in the transverse plane is determined by an optical Glauber parametrization [5] and the parameters of the calculation, namely the equilibration time $\tau_{\rm equ}$ and the constant $s_{\rm equ}$ which relates the geometrical density to the initial entropy density are obtained by fitting to preliminary particle spectra from central Au+Au collisions with $\sqrt{s_{\rm NN}} = 200$ GeV. Good agreement is achieved with $s_{\rm equ} = 110$ fm$^{-3}$ at $\tau_{\rm equ} = 0.6$ fm/$c$ [6], to be used in the following.

**Evolution of entropy and temperature:** We first study the time evolution of the entropy density and the temperature at the center of the system and at 3 and 5 fm radial distance (Fig. 1). Initially the entropy decays with a $\tau^{-1}$ power law due to the initial longitudinal Bjorken expansion (see the dashed lines). As time evolves, the transverse pressure gradients lead to a collective radial expansion and thus a transition from the initial one-dimensional to a full three dimensional expansion in the late stage. At late times the dashed line indicates a decay $\sim\tau^{-3}$.

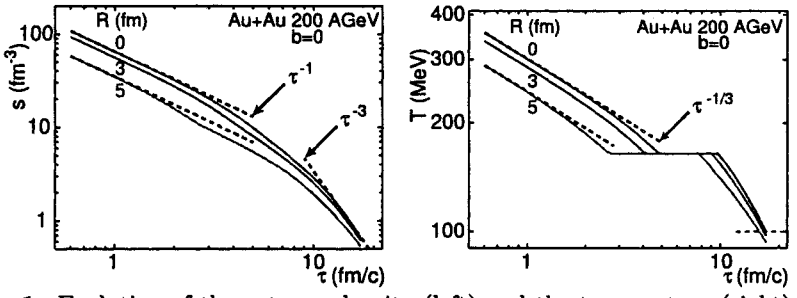


**Fig. 1.** Evolution of the entropy density (left) and the temperature (right) for central Au+Au collisions at $\sqrt{s_{\rm NN}} = 200$ GeV. Shown are the densities and temperatures at distances $R = 0$, 3 and 5 fm from the center of the system

The equation of state supplemented to the hydrodynamic equations of conservation of energy and momentum features a strong first order phase transition at a critical temperature of $T_c = 164$ MeV. Above that temperature the system acts like an ideal gas with $c_s^2 = \partial p/\partial e = 1/3$ and $e \sim T^4$. For a one-dimensional Bjorken expansion the energy density decays as $e \sim \tau^{-(1+c_s^2)}$ and thus $T \sim \tau^{-1/3}$. The figure shows that this behavior is neatly followed until just before the system hits the mixed phase where the temperature remains unchanged while the system boils off its latent heat. Further cooling appears then in the resonance gas phase below $T_c$.

**Evolution of radial velocity:** Now we consider the collective radial velocity which is generated through the act of the pressure gradients in the system. The left plot of Fig. 2 shows the radial flow velocity at distance 3 and 5 fm from the fireball center. As pressure gradients are larger at 5 fm than at 3 fm, the acceler-

ation is stronger and thus the rise of $v_r(\tau)$. When the system reaches the mixed phase, the acceleration ceases and the velocity locally drops as matter continues to move radially outward, thus transporting the slower fluid cells from the interior to larger radial distances. Only as the matter cools into the hadronic phase, pressure gradients pick up again and more radial flow is generated.

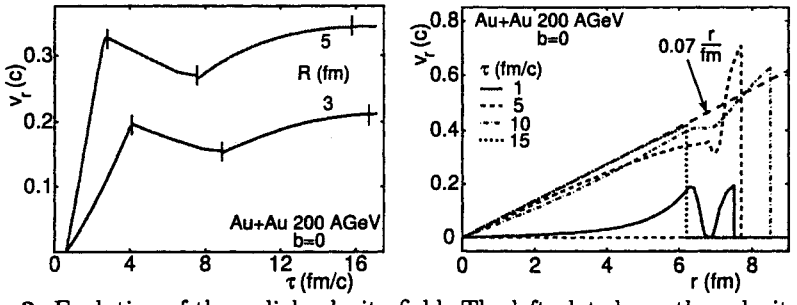


**Fig. 2.** Evolution of the radial velocity field. The left plot shows the velocity as a function of time at positions 3 and 5 fm away from the center of the system. The right plot shows the radial flow profile as a function of the radial distance at 4 different times together with a linear relation $v_r = \xi r$ with $\xi = 0.07$ fm$^{-1}$

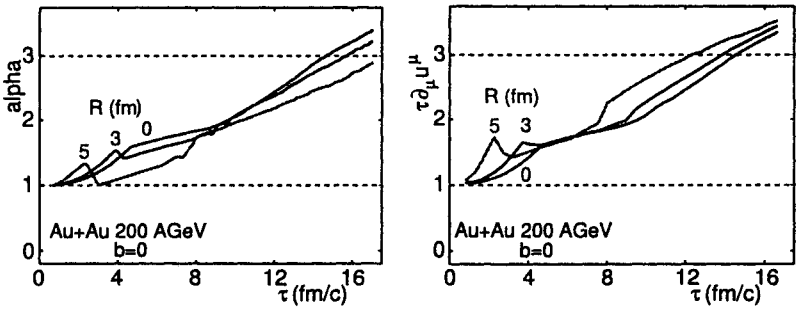


**Fig. 3.** Evolution of the local expansion parameter $\alpha$ and the product of expansion rate and time, $\tau\,\partial_\mu u^\mu$ at distances $R = 0$, 3 and 5 fm from the center

The right hand plot of Fig. 2 shows the radial flow field as a function of radial distance at four different times. The generated flow field 1 fm/$c$ after impact has an interesting structure, showing a non-monotonous behavior due to the mixed phase where no collective flow develops. As time evolves the field rapidly adopts a linear behavior which is largely preserved for the rest of the evolution, and can very well be described by $v_r(r) = \xi r$ ($\approx \tanh(\xi r)$) with $\xi = 0.07$ fm$^{-1}$. This 'static' flow field is at the heart of the successful description of a large number of observables in terms of the popular 'blast wave' parametrization [7].

**Evolution of dilution and expansion rates:** We now return to the dilution and expansion rates in the full hydrodynamic calculation. Figure 3 shows the evolution of the local expansion parameter $\alpha = -(\tau/s)(\partial s/\partial\tau) = -(\partial \log s)/(\partial \log \tau)$ in the left panel. It is clearly seen how the initial one-dimensional motion with $\alpha = 1$

becomes more three-dimensional and just reaches $\alpha = 3$ at the time of decoupling (assuming freeze-out at $T_d = 100$ MeV). Note the influence of the radial position during late stages of the expansion. At larger radial distances the dilution rate is smaller, as supplies from the interior are constantly streaming outward.

The right panel of the figure shows the evolution of the product of expansion rate and time, $\tau\, \partial_\mu u^\mu$. Note that with increasing the radial distance we get an opposite behavior as exhibited by the dilution rate. As demonstrated by the analytical calculation before, the expansion rate increases with radial distance. The sign of the difference is understood in terms of Eq. (3).

## 4. Time Evolution of Anisotropies in Non-Central Collisions

Observables from non-central collisions deliver the strongest arguments for rapid thermalization and a subsequent hydrodynamic expansion of the reaction region [8]. The geometric anisotropy in non-central collision $\epsilon_x$ results in anisotropic pressure gradients which in turn lead to anisotropies in the collective flow field. Those can be characterized in terms of $\epsilon_p$, the asymmetry of the transverse part of the energy momentum tensor [4]. This flow anisotropy will finally be observable as an azimuthal dependence of particle emission (i.e. elliptic flow) [9]. From the left part of Fig. 4, which shows contours of constant energy density in the transverse plane at different times, it can be seen how the initial spatial eccentricity quickly diminishes. This becomes more quantitative in the right part of the figure where the evolution of $\epsilon_x$ and $\epsilon_p$ for a system with (RHIC 1) and without (EOS I) a first order phase transition is shown. The large initial geometric eccentricity leads to a rapid generation of momentum anisotropy, which in turn reduces the spatial eccentricity, and thus cuts off the further generation of momentum anisotropy. During the soft phase of the transition pressure gradients vanish (and thus also their anisotropies),

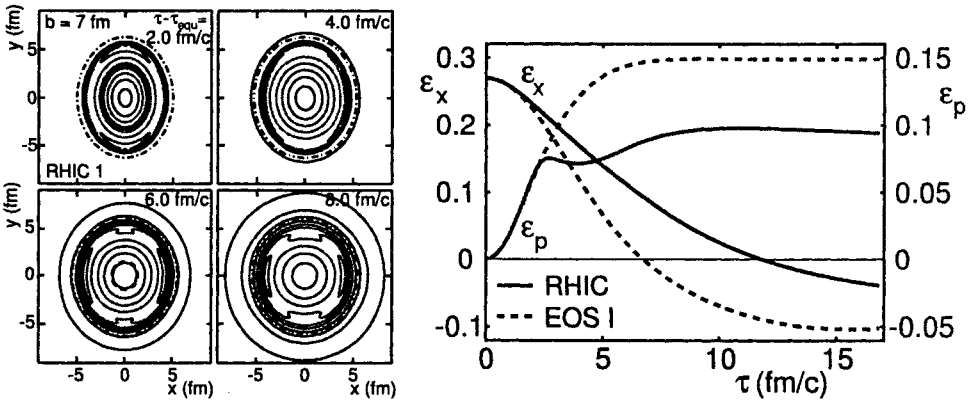


**Fig. 4.** Contours of the energy density in the transverse plane at four different times during the systems' evolution. The figure to the right shows the time evolution of the spatial eccentricity $\epsilon_x$ and the momentum anisotropy $\epsilon_p$, for a system with (RHIC 1) and without (EOS I) a phase transition

which leads to an even earlier saturation of the momentum anisotropy. For systems at RHIC most of the anisotropy is thus generated in the plasma stage of the fireball.

## 5. Summary and Relevance

We have given a detailed account on the evolution of the thermodynamic fields in systems created at RHIC within a hydrodynamic framework. This information is relevant for the microscopic dynamics at different levels. At early stages, hard probes are to be transported over the varying thermodynamic background fields to calculate their energy loss. At late stages, the scattering rates in the resonance gas needs to be compared to the macroscopic expansion and dilution rates to investigate the overall reliability of the idealized macroscopic approach which requires a 'slow' (adiabatic) evolution and strong rescattering. Furthermore there are sensitive probes of the density around decoupling such as light nuclei, whose formation probability favors a large density, but their survival rate increases with decreasing density. Resonances reconstructed from a hadronic decay channel have similar information content [10]. In summary, essentially all experimental observables are influenced by the temporal evolution of the thermodynamic fields presented here either as the signal is sensitive to all stages of the evolution and thus integrates the temporal history of the system or as it results from a particular stage of the collision with densities and their gradients giving the relevant physical background.

## Acknowledgments

This research was supported in part by the U.S. Department of Energy under Grant No. DE-FG02-88ER40388. Support from the Alexander von Humboldt Foundation through a Feodor Lynen Fellowship is gratefully acknowledged.

## References

1. *Proc. of the 15th and 16th Int. Conf. on Ultrarelativistic Nucleus–Nucleus Collisions*, *Nucl. Phys.* **A698** (2002) 1c; ibid. **A715** (2003) 1c.
2. P.F. Kolb and U. Heinz, nucl-ex/0305084.
3. B. Tomasik and U. Wiedemann, nucl-th/0207074.
4. P.F. Kolb, J. Sollfrank and U. Heinz, *Phys. Rev. C* **62** (2000) 054909.
5. P.F. Kolb, U. Heinz, P. Huovinen, K.J. Eskola and K. Tuominen, *Nucl. Phys.* **A696** (2001) 197.
6. P.F. Kolb and R. Rapp, *Phys. Rev. C* **67** (2003) 044903.
7. E. Schnedermann, J. Sollfrank and U. Heinz, *Phys. Rev. C* **48** (1993) 2462.
8. P.F. Kolb et al., *Phys. Lett.* **B500** (2001) 232; P. Huovinen et al., *Phys. Lett.* **B503** (2001) 58; D. Teaney et al., *Phys. Rev. Lett.* **86** (2001) 4783; T. Hirano, *Phys. Rev. C* **65** (2001) 011901(R).
9. J.-Y. Ollitrault, *Phys. Rev. D* **46** (1992) 229.
10. G.E. Brown and E.V. Shuryak, *Nucl. Phys.* **A717** (2003) 322; P.F. Kolb and M. Prakash, *Phys. Rev. C* **67** (2003) 044902.